Robust room-temperature magnetism of (110) CrO_2 thin films

Manjit Pathak,[1,2] Hunter Sims,[1,2] Krishna B. Chetry,[1,2] Dipanjan Mazumdar,[2] Patrick R. LeClair,[1,2] Gary J. Mankey,[1,2] William H. Butler,[1,2] and Arunava Gupta[2,3]

[1]*Department of Physics and Astronomy, University of Alabama, Tuscaloosa, Alabama 35487, USA*

[2]*MINT Center, University of Alabama, Tuscaloosa, Alabama 35487, USA*

[3]*Department of Chemistry, University of Alabama, Tuscaloosa, Alabama 35487, USA*

(Received 26 October 2009; published 14 December 2009)

We have used x-ray magnetic circular dichroism (XMCD) and *ab initio* electronic-structure calculation techniques to investigate the magnetic properties of high-quality epitaxial (110) and (100) CrO_2 thin films. A relatively larger XMCD was observed on the Cr $L_{2,3}$ edge of (110)-oriented CrO_2 films compared to (100)-oriented CrO_2 films at room temperature. Analysis of our data with conventional sum rules for 3*d* elements shows a nearly 50% higher spin moment on (110) films compared to (100) orientation, consistent with bulk magnetometry measurements. The orbital moment is found to be similar for both orientations. Robust magnetism is attributed to increased collinearity of Cr spins in strain-free (110) films as compared to strained (100) films. Zero-temperature density-functional calculations show opposing trends in nearest-neighbor and next-nearest-neighbor exchange interactions between relaxed and strained CrO_2.

DOI: 10.1103/PhysRevB.80.212405 PACS number(s): 75.10.−b, 31.15.A−, 75.70.−i

CrO_2 is a well-established half metal. Point-contact Andreev reflection[1–4] and Meservey-Tedrow spin-polarized tunneling measurements[5] on CrO_2 have recorded spin-polarization values as high as 98%. Half metallicity makes CrO_2 one of the most attractive candidates for spin-electronic devices since very large tunnel or giant magnetoresistance can, in principle, be obtained with CrO_2-based devices. Other properties of CrO_2 include its selective growth on patterned TiO_2 substrates,[6] columnar growth on Al_2O_3 substrates,[7] and controlled magnetic and transport properties by substrate-induced stress.[8,9]

The enormous potential of CrO_2 is still untapped since its interface/surface properties—and the various factors affecting them—are relatively unknown. One crucial aspect that is relatively unexplored is the influence of strain on the properties of CrO_2 thin films and devices. Previously, it was shown that (100) CrO_2 films grown on isostructural (100) TiO_2 substrates are significantly strained even for films thicker than 200 nm, resulting in a strong temperature dependence of the magnetocrystalline anisotropy.[8] As shown in Fig. 1(a), (100) CrO_2 films on TiO_2 substrates are under compressive strain along the out-of-plane (010) direction, i.e., along the *b* axis, and under tensile strain along in-plane directions (*a* and *c* axes). This strain is due to substrate-induced stress because the TiO_2 unit cell is larger than the CrO_2 unit cell in the *a*, *b*, and *c* directions. The magnetic easy axes of such films were found to gradually rotate upon cooling from the *c*-axis (300 K) to *a*-axis (10 K) direction.[8] In contrast, our recent x-ray diffraction studies on (110) CrO_2 films, on the other hand, showed relatively strain-free film growth for thicknesses as low as a few tens of nanometers.[10] As shown in Fig. 1(b), (110) CrO_2 films grow strain free in all directions. While the growth mechanisms are still under investigation, surface-energy differences between TiO_2 and CrO_2 are believed to promote an island growth mode for (110) CrO_2 leading to strain-free film.[10] Bulk magnetic properties of (110)-oriented films show higher magnetocrystalline anisotropy and no easy-axis variation with temperature—pointing to their substantially different material properties.

In this paper we investigate the surface magnetic properties of (110) and (100) CrO_2 thin films using the element-specific and surface/interface sensitive x-ray magnetic circular dichroism (XMCD) technique. (110)-oriented CrO_2 films show substantially stronger XMCD than (100) films at room temperature which we quantify using the XMCD sum rules.[11] We find the room-temperature magnetism of (100) films to be significantly suppressed—almost 50% lower compared to (110) films. This result is supported by temperature-dependent bulk magnetization measurements. Orbital moments, on the other hand, show no substantial difference between the two orientations. We have also performed *ab initio* calculations to investigate the effect of strain on exchange interactions of CrO_2.

For our experiment, CrO_2 samples of both (100) and (110) orientations were deposited on TiO_2 substrates of the same respective orientations by a standard chemical vapor deposition technique using a solid CrO_3 precursor.[12] Growth details

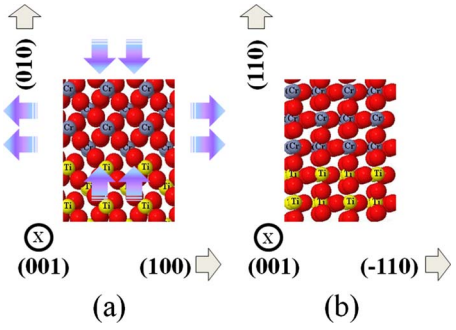

FIG. 1. (Color online) Rutile structure of (100)- and (110)-oriented CrO_2 films are shown in (a) and (b), respectively, on TiO_2 substrates of respective orientations. Unlabeled spheres indicate the O^{2-} ions on both structures. Out-of-plane directions on (100) and (110) films are (010) and (110), respectively, as shown in the figure. In the (100) structures, compressive strain along out-of-plane direction and tensile strain along in-plane directions are schematically shown while the (110) structure remains strain free.

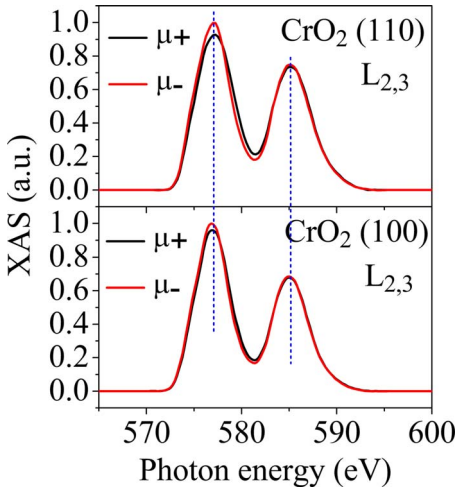

FIG. 2. (Color online) Photon-energy scan on Cr $L_{2,3}$ edges (600–565 eV), showing strong polarization-dependent x-ray absorption. We observed Cr L_2 and L_3 peaks at 585 and 577 eV, respectively, within the resolution of the instrument (± 0.25 eV) for both (100) and (110) oriented films. XAS data are normalized for comparison between the spectra of (100) and (110) oriented films.

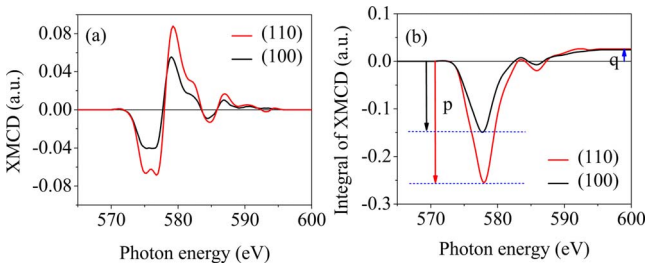

FIG. 3. (Color online) (a) XMCD, i.e., $(\mu_+ - \mu_-)$ is shown in figure (a) obtained from the XAS on (100) and (110) films of CrO_2 and figure (b) shows the integral of XMCD. Here $p = \int_{L_3}(\mu_+ - \mu_-)d\omega$ and $q = \int_{L_2+L_3}(\mu_+ - \mu_-)d\omega$, obtained by integration of the XMCD signal. The quantity $r = \int_{L_2+L_3}(\mu_+ + \mu_-)d\omega$ in the sum-rule analysis is calculated from the integral of summing over the XAS signal (not shown).

are reported in a previous publication.[10] All films had thicknesses of ~45 nm, accurately measured by grazing incidence x-ray reflectivity using a Philips X'pert Diffractometer. Atomic force microscopy performed on as-grown samples shows our films to be extremely flat, with rms roughness of less than 1.0 nm (figure not shown). XMCD experiments were carried out on *port 123*, 10 m toroidal grating monochromator at the Synchrotron Radiation Center (SRC) at the University of Wisconsin, Madison. In the XMCD setup, polarized soft x rays (~85% polarization) were incident at an angle of $45° \pm 5°$ relative to the sample surface, parallel to the *c* axis of CrO_2, and all spectra were collected by the total electron yield method at room temperature with an energy resolution of 0.25 eV. The photon helicity was fixed and the film magnetization was switched by applying a ± 1400 Oe magnetic field along the easy "*c*" axis to obtain the XMCD spectra. An average of at least five spectra is reported here. The effect of strain on the exchange energy of CrO_2 was evaluated by performing first-principles calculations within density-functional theory[13] and the generalized gradient approximation (GGA) (Ref. 14) using the Vienna *ab initio* simulation package (VASP) (Refs. 15–18) and pseudopotentials generated by Kresse and Joubert.[19] For structural-relaxation and constrained-field calculations (explained later), a $9 \times 5 \times 15$ Monkhorst-Pack *k*-point mesh was used for the supercell with cells stacked along the *b* axis, and a $9 \times 9 \times 7$ mesh was used for the supercell aligned along the *c* axis. Forces were relaxed to less than (0.01 eV/Å) and an energy cutoff of 500 eV was used for the plane-wave expansion of the projector augmented wave.

In Fig. 2 we show the normalized x-ray absorption (XAS) spectra of (110) and (100) CrO_2 films on Cr $L_{2,3}$ edges after saturating the films in opposite directions with fixed photon helicity (indicated by μ_+ and μ_-). We also obtained XAS spectra on the O-*K* edge, scanning the beam energy from 550 to 515 eV. However, no unambiguous XMCD was observed from the O-*K* edge at room temperature. Therefore, in our analysis we have neglected any spin and orbital contribution coming from the O^{2-} ions in CrO_2. In Fig. 3(a), we plot the XMCD spectra which is obtained by subtracting the two XAS spectra obtained at opposite sample magnetizations. The (110)-oriented films show a larger XMCD signal than (100) films, as evidenced by the stronger peaks at the L_3 edge. The XMCD line shapes are nearly identical and agree well with previous results obtained on (100)-oriented films near room temperature.[20] Quantitative analysis using the sum rules for 3*d* elements is somewhat complicated for transition-metal oxides in general and for CrO_2 in particular.[23] Two main issues are relevant in the case of CrO_2. The first arises from the weak spin-orbit splitting of the Cr 2*p* levels and the second from the distorted oxygen octahedra around the central Cr^{4+} ion. Weak spin-orbit coupling leads to substantial "spectral overlap," meaning that the $2p_{3/2}$-3*d* (L_3) and $2p_{1/2}$-3*d* (L_2) transitions lie very close in energy. This overlap has been estimated to give 5–15 % error in the sum rules.[21] Additionally, and more importantly, the x-ray absorption is not from pure $p_{3/2}$ or $p_{1/2}$ states but rather from a quantum-mechanical superposition of both. This is commonly referred to as jj mixing. To take into account this mixture, correction factors have been evaluated for some systems and estimated to be approximately 2.0 for bulk Cr and we use this value in our estimates.[21] Complications from the distorted CrO_2 octahedra result in a substantial contribution to the dipole-moment term, represented by T_z in the spin sum rule. This T_z term for CrO_2 has been reported to be much larger than that for 3*d* metals such as Fe, Co, and anisotropic.[22] In our calculations, for a lack of proper understanding and available data, we do not correct for the T_z value and further assume the T_z value to be the same for (100) and (110) orientations as the c/a ratio values are found to be 0.669 for strained (100) structure and 0.659 for the strain-free (110) structure suggesting a small tetragonal distortion due to strain in (100) structure. The orbital moment, on the other hand, does not depend on the T_z term explicitly and can be estimated directly using the sum rules.

Knowing these limitations, we analyzed our data using the XMCD sum rules for 3*d* elements.[11] To be more specific, we evaluated the XMCD integral over the L_3 edge (*p*), the

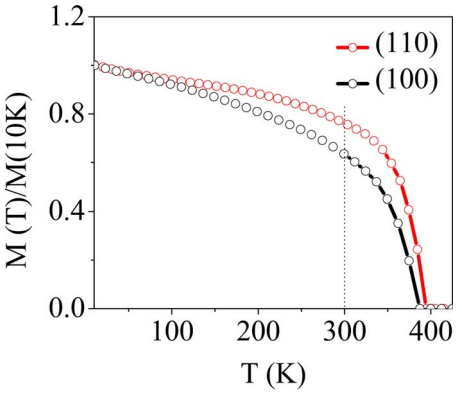

FIG. 4. (Color online) Normalized magnetic moments of (100) and (110) CrO_2 films plotted vs temperature in steps of 10 K. Data from 10 to 350 K were taken in SQUID and from 300 to 425 K were taken using a VSM. No offset in moment was found between SQUID and VSM data. Moment values are estimated to be correct within less than 2% of their measured value at all temperatures and temperature was stable within 0.2 K. The T_c for (100) and (110) CrO_2 films are found to be 385 and 393 K, respectively. Considering the fluctuations near T_c, the error in T_c can be estimated to be ± 5 K.

combined integral over L_3 and L_2 edges (q), and separately the background corrected XAS spectra over the L_3 and L_2 edges (r). We use $N_{3d}=8.0$ for Cr^{4+}, and knowing these values the sum rules take a simpler form: $m_s+7T_z=2^*(4q-6p)/r$ and $m_l=-8q/3r$. In Fig. 3(b), we plot the sum integrals p and q vs energy (r not shown). We find the orbital moment to be virtually identical for both (100) and (110) orientations, approximately $(-0.030\pm0.005)\mu_B$. This value agrees reasonably well with LDA+U calculations of Komelj *et al.*[23] ($-0.037\mu_B$) but is slightly lower than experimental reports of Goering *et al.*[22] ($-0.062\mu_B$) and Huang *et al.*[24] ($-0.051\mu_B$). The spin moments were found to be $(1.2\pm0.2)\mu_B$ and $(1.8\pm0.3)\mu_B$ for (100) and (110) orientations, respectively. Since these measurements are at room temperature, we expect the moment values to be less than $2.0\mu_B$ per Cr, the experimental and theoretical bulk moment at low temperature, consistent with a $3d^2$ electronic configurations for Cr^{4+} ion.

We therefore find the (110) spin moment to be nearly 50% higher than (100) orientation at room temperature. This is consistent with bulk magnetic measurements shown in Fig. 4 measured using a Quantum Design superconducting quantum interference device (SQUID) system and vibrating sample magnetometer (VSM). Temperature scans of the magnetic moment for both films are shown in Fig. 4. Magnetization for both films at 10 K is found to be $\sim 6.5\times10^5$ A/m which is in agreement with previous reported magnetization values at low temperature.[8] However, the magnetic moment decays faster in case of (100) CrO_2 films which are about 25% lower than (110) CrO_2 films at room temperature though SQUID and VSM measure the total magnetic moment of the film while XMCD gives surface magnetic moment. Given the 10–15 % error in moment estimation with XMCD, the difference in moment between (100) and (110) CrO_2 films at room temperature obtained by SQUID is in good agreement with the difference calculated from XMCD analysis. We believe this is an intrinsic property of our high-quality CrO_2 thin films, and a direct manifestation of the different effects of strain in the two orientations. As supporting evidence, Fig. 4, the Curie temperature (T_c) for (100) CrO_2 was found to be slightly lower than that of (110) CrO_2. It is known that T_c can be suppressed due to strain[25] in a film.

In order to understand the experimental results, we performed first-principles calculations of the electronic structures of unstrained and strained CrO_2 using density-functional theory[13] in the GGA (Ref. 14) as implemented in the VASP code.[15–18] To model the strained cell, the in-plane lattice constant values (a and c) of TiO_2 and the experimental out-of-plane value (b axis) of CrO_2 from Ref. 10 were used. The internal coordinates of the ions were relaxed starting from the GGA-relaxed CrO_2 value for this calculation. This strained structure was found to be half metallic (online information) with a zero-temperature moment of $2\mu_B$/f.u.—consistent with a Cr^{4+} configuration and similar to bulk CrO_2 calculations. The density of states analysis showed an overall slight upward shift for the Cr $3d$ and O $2p$ bands (online information), consistent with the higher electronic energy of this structure (online information). Next we evaluated the nearest-neighbor exchange constant (J_1) along the body-diagonal (111) direction and the next-nearest-neighbor exchange constants (J_2) along c (001) and b (010) directions of the CrO_2 cell. For reference, along with the strained cell, we have also calculated the exchange constants for the GGA-relaxed configuration and the experimental bulk structure (results summarized in Table I). To accomplish this calculation, a series of constrained-field calculations were performed within an internally relaxed 12-atom supercell using the method outlined in Ref. 26. In short, the total electronic energy was calculated with the magnetic moment of selected Cr ions rotated up to 60° (noncollinear configuration), and the energy vs angle data fitted to a Heisenberg model to determine the exchange constants. This analysis showed two contrasting trends. We found a small reduction

TABLE I. The nearest- and next-nearest-neighbor exchange constants for the experimental bulk, GGA-relaxed, and the experimental strained rutile CrO_2 cell.

Structure	Lattice constants (Å)	Volume (Å^3)	J_1 (111) (meV)	J_2 (010) (meV)	J_2 (001) (meV)
Expt. Bulk	$a=b=4.421$, $c=2.916$	56.994	23.2	−11.8	33.8
GGA Bulk	$a=4.451$, $b=4.448$, $c=2.923$ (+0.67%, +0.60%, +0.24%)	57.869	22.9	−10.4	35.8
Expt. Strained	$a=4.584$, $b=4.377$, $c=2.958$ (+3.69%, −1.00%, +1.44%)	59.349	22.5	−8.1	40.1

in J_1 in the strained cell (22.5 meV) compared to the GGA-relaxed (22.9 meV) and the experimental-relaxed (23.2 meV) configurations. This is consistent with the picture that the distance between the body-center and corner Cr ions increases in the strained cell. But we also observe a substantial increase in J_2 both along (001) and (010) directions as outlined in Table I. Overall this latter effect dominated the total exchange energy. Therefore, our zero-temperature calculations indicate that the Curie temperature of the strained cell should be higher than either the GGA relaxed or the experimental bulk structure—in contradiction to experimental results. The increase in J_2 along the c direction is particularly striking. The physical reason for such a behavior is not understood at this moment and shall be a subject of future investigation. It should be emphasized that the theoretical calculations are at zero temperature whereas the experimental deviation in the magnetization between strained and strain-free CrO_2 are pronounced near room temperature. Second, it is plausible that J_1 and J_2 have different temperature dependence with J_1 dominating J_2 as we approach the Curie temperature. Also it should be pointed out that for our 0 K calculations we have used the available room-temperature lattice-constant values. Additionally, during the course of our calculation we found the exchange energy to extremely sensitive to the internal parameters (particularly the oxygen positions). These values were not available for the strained structure. Therefore, we speculate that the discrepancy between theory and experiment could originate from one or all of the above-mentioned possibilities.

In conclusion, we carried out XMCD measurements on CrO_2 thin films of (100) and (110) orientations at room temperature and analyzed the data using XMCD sum rules. Spin moments were found to be almost 50% higher for (110)-oriented films compared to (100)-oriented films. Temperature-dependent bulk magnetometry measurements revealed a similar trend with (100) films also exhibiting a slightly lower Curie temperature. We attribute these effects to the intrinsically different growth modes of (100) and (110) films on TiO_2 substrates; (100) films grow strained while (110) films grow strain free. Orbital moments were found to be the same for both orientations. Zero-temperature calculations of the nearest- and next-nearest-neighbor exchange constants using density-functional methods were found to be extremely sensitive to the lattice parameters. For the relaxed and the strained structures that were considered, an overall increase in exchange energy originating from strong next-nearest interactions was found in the strained cell, masking a small reduction in nearest-neighbor exchange.

The authors gratefully acknowledge Mary Severson and Mark Bissen for helping with beam line and troubleshooting during experiment. Authors also gratefully thank E. Goering of Max-Plank-Institute für Metallforschung, Stuttgart, Germany for fruitful suggestions and discussions. Hideo Sato's help with detailed x-ray analysis of our samples and Gihan Kwon's help with data analysis are also gratefully appreciated. This work is based in part upon research conducted at the Synchrotron Radiation Center, University of Wisconsin-Madison, which is supported by the National Science Foundation under Award No. DMR-0537588. This work has been supported by funding from NSF under Grant No. DMR-0706280.

[1] S. K. Upadhyay, A. Palanisami, R. N. Louie, and R. A. Buhrman, Phys. Rev. Lett. **81**, 3247 (1998).
[2] A. Anguelouch, A. Gupta, G. Xiao, D. W. Abraham, Y. Ji, S. Ingvarsson, and C. L. Chien, Phys. Rev. B **64**, 180408(R) (2001).
[3] J. S. Parker, S. M. Watts, P. G. Ivanov, and P. Xiong, Phys. Rev. Lett. **88**, 196601 (2002).
[4] Y. Ji, G. J. Strijkers, F. Y. Yang, C. L. Chien, J. M. Byers, A. Anguelouch, G. Xiao, and A. Gupta, Phys. Rev. Lett. **86**, 5585 (2001).
[5] R. Meservey and P. M. Tedrow, Phys. Rep. **238**, 173 (1994).
[6] A. Gupta, X. Li, S. Guha, and G. Xiao, Appl. Phys. Lett. **75**, 2996 (1999).
[7] M. Rabe, J. Pommer, K. Samm, B. Ozyilmaz, C. Konig, M. Fraune, U. Rudiger, G. Guntherodt, S. Senz, and D. Hesse, J. Phys.: Condens. Matter **14**, 7 (2002).
[8] G. Miao, G. Xiao, and A. Gupta, Phys. Rev. B **71**, 094418 (2005).
[9] X. W. Li, A. Gupta, and G. Xiao, Appl. Phys. Lett. **75**, 713 (1999).
[10] K. B. Chetry, M. Pathak, P. LeClair, and A. Gupta, J. Appl. Phys. **105**, 083925 (2009).
[11] C. T. Chen, Y. U. Idzerda, H. J. Lin, N. V. Smith, G. Meigs, E. Chaban, G. H. Ho, E. Pellegrin, and F. Sette, Phys. Rev. Lett. **75**, 152 (1995).
[12] S. Ishibashi, T. Namikawa, and M. Satou, Mater. Res. Bull. **14**, 51 (1979).
[13] W. Kohn and L. J. Sham, Phys. Rev. **140**, A1133 (1965).
[14] Y. Wang and J. P. Perdew, Phys. Rev. B **43**, 8911 (1991).
[15] G. Kresse and J. Hafner, Phys. Rev. B **47**, 558 (1993).
[16] G. Kresse and J. Hafner, Phys. Rev. B **49**, 14251 (1994).
[17] G. Kresse and J. Furthmüller, Comput. Mater. Sci. **6**, 15 (1996).
[18] G. Kresse and J. Furthmüller, Phys. Rev. B **54**, 11169 (1996).
[19] G. Kresse and D. Joubert, Phys. Rev. B **59**, 1758 (1999).
[20] S. Gold, E. Goering, C. Konig, U. Rudiger, G. Guntherodt, and G. Schutz, Phys. Rev. B **71**, 220404(R) (2005).
[21] E. Goering, Philos. Mag. **85**, 2895 (2005).
[22] E. Goering, A. Bayer, S. Gold, G. Schutz, M. Rabe, U. Rudiger, and G. Guntherodt, Phys. Rev. Lett. **88**, 207203 (2002).
[23] M. Komelj, C. Ederer, and M. Fähnle, Phys. Rev. B **69**, 132409 (2004).
[24] D. J. Huang, H. T. Jeng, C. F. Chang, G. Y. Guo, J. Chen, W. P. Wu, S. C. Chung, S. G. Shyu, C. C. Wu, H. J. Lin, and C. T. Chen, Phys. Rev. B **66**, 174440 (2002).
[25] A. J. Millis, T. Darling, and A. Migliori, J. Appl. Phys. **83**, 1588 (1998).
[26] H. Sims, S. J. Oset, W. H. Butler, James M. McLaren, and Martijn Marsman (unpublished).